Research Square

Preprints are preliminary reports that have not undergone peer review.
They should not be considered conclusive, used to inform clinical practice,
or referenced by the media as validated information.

A Stress-Based Prediction of Support Failure and Its Influence on Machining Quality in Support-Assisted Milling of LPBF Parts

Min Ji Ham
Korea Institute of Industrial Technology
Seung Jun Han
Korea Institute of Industrial Technology
Won Rae Kim
Korea Institute of Industrial Technology
Gun-Hee Kim
Korea Institute of Industrial Technology
Bo Hyun Kim
Soongsil University
In Yong Moon
mooniy085@kitech.re.kr

Korea Institute of Industrial Technology

Research Article

Keywords: Laser powder bed fusion, Support structure, Milling, Max principal stress, Post process, Finite Element Analysis

Posted Date: July 13th, 2026

DOI: https://doi.org/10.21203/rs.3.rs-10037118/v1

License: This work is licensed under a Creative Commons Attribution 4.0 International License.
Read Full License

Additional Declarations: No competing interests reported.

Version of Record: A version of this preprint was published at Progress in Additive Manufacturing on October 21st, 2026. See the published version at https://doi.org/10.1007/s40964-026-02010-1.

A Stress-Based Prediction of Support Failure and Its Influence on Machining Quality in Support-Assisted Milling of LPBF Parts

Laser powder bed fusion (LPBF) enables the fabrication of complex metallic components; however, milling-based post-processing is required to achieve functional surface quality and dimensional accuracy. Once separated from the build plate, the fabricated part must be re-fixed to a milling machine using additional clamping fixtures, and this procedure increases process complexity and machining errors due to repeated setup and alignment. To address this limitation, this study proposes a stress-based design approach for utilizing as-built support structures as structural fixtures during support-assisted milling. Cutting forces of LPBF-fabricated Pure Titanium specimens were experimentally measured under various machining conditions, and a mechanistic load model was established. The derived load model was used to estimate cutting loads for different process parameters. Support-assisted milling experiments were conducted to observe structural behavior and identify the onset of support failure under increasing cutting loads. Finite element simulations were performed using the calculated cutting loads to evaluate stress distributions within the support structures. For each design variable, the critical maximum principal stress corresponding to failure initiation was determined. Validation using a complex cage geometry demonstrated that the proposed stress criterion reliably predicts machining stability. The influence of stress levels on machining quality was further examined. Even below the critical stress threshold, increasing stress resulted in gradual deterioration of straightness error and surface roughness, indicating that stress magnitude affects machining performance prior to structural failure. The proposed approach provides a quantitative framework linking cutting load, stress distribution, failure initiation, and machining quality, thereby enabling predictive evaluation of support-assisted milling feasibility prior to machining.

Keywords: Laser powder bed fusion, Support structure, Milling, Max principal stress, Post process, Finite Element Analysis

1. Introduction

Additive manufacturing (AM) enables the direct fabrication of components with complex geometries and internal structures, and its application has rapidly expanded across high-value industries such as aerospace, biomedical engineering, and defense [1-5]. Among various AM technologies, Laser powder bed fusion (LPBF) has been widely adopted for structural applications due to its ability to selectively melt and consolidate metal powders using a high-energy laser, producing components with high density and favorable mechanical properties [2,4,5].

Despite these advantages, LPBF processes inherently suffer from limitations associated with rapid melting and solidification, including surface roughness, dimensional deviations, and residual stress accumulation [4-6]. As a result, as-built components often fail to meet the dimensional accuracy and surface integrity required for functional applications, making milling-based post-processing essential [7-11].

The importance of post-processing becomes even more pronounced for additively manufactured medical components. In particular, medical devices such as patient-specific implants require complex geometries and high dimensional accuracy, making precision machining an essential post-processing step. Pure Ti Grade 2 is one of the most widely used metallic materials for such applications due to its excellent biocompatibility and corrosion resistance. Furthermore, medical AM components are typically characterized by low-volume, high-customization production, making the efficiency of post-processing operations a critical factor in overall manufacturing performance. Therefore, there is an increasing demand for post-processing strategies that can simultaneously improve machining accuracy and manufacturing efficiency.

In current industrial practice, LPBF-fabricated parts typically undergo a sequence of post-processing steps including heat treatment, separation from the build plate, support removal, fixture design and fabrication, clamping, and re-establishment of machining reference coordinates. This workflow involves multiple setup operations and repeated alignment procedures, which increase process complexity and introduce potential positioning errors that directly affect machining quality. The challenge becomes more significant for geometrically complex parts, where limited machining accessibility and fixture design difficulties further reduce manufacturing efficiency.

Support structures generated during LPBF are indispensable for providing geometric support and heat dissipation during fabrication [12-14]. However, they have traditionally been regarded as sacrificial elements to be removed

after printing. The potential of utilizing support structures as structural fixtures during post-machining has received limited attention. If support structures could be retained and used directly as clamping fixtures during milling, additional fixture fabrication and coordinate re-alignment could be eliminated, enabling a more integrated manufacturing workflow between AM and subtractive processing.

Previous studies have explored concepts such as direct machining of additively manufactured parts and the dynamic behavior of part–build plate integrated systems [10,15-17]. Nevertheless, most existing work has focused on vibration response, displacement behavior, or stability lobe prediction [18-21]. Quantitative design criteria that directly correlate milling-induced stresses within support structures to structural failure have not been clearly established. Moreover, the relationship between stress levels in support structures and machining quality degradation has not been systematically investigated. Consequently, support structures remain treated primarily as temporary sacrificial components rather than as functional design variables in process planning.

Structural failure of support elements is expected to initiate in regions where stress concentration occurs, particularly under maximum principal stress. Therefore, a maximum principal stress-based approach provides a physically meaningful criterion for predicting structural failure. While displacement- or vibration-based analyses are useful for evaluating machining stability, a stress-based criterion offers a more direct indicator for assessing the structural integrity of support structures. From this perspective, a stress-based design framework is essential for redefining support structures as functional process elements.

This study proposes a maximum principal stress-based strategy for predicting support failure in support-assisted milling, where support structures are retained and utilized as clamping fixtures (Fig. 1). Cutting forces of LPBF-fabricated Pure titanium (Ti) Grade 2 specimens were experimentally characterized under various machining conditions, and a mechanistic load model based on cutting cross-sectional area was established [22-25]. A series of specimens incorporating different support design parameters were fabricated, and support-assisted milling experiments were conducted to identify critical machining conditions associated with support failure. Finite element analysis (FEA) was performed under identical loading conditions to evaluate stress distributions and determine critical stress values for each support configuration. Finally, the influence of stress level on machining quality was examined to assess the applicability of the proposed stress-based design criterion.

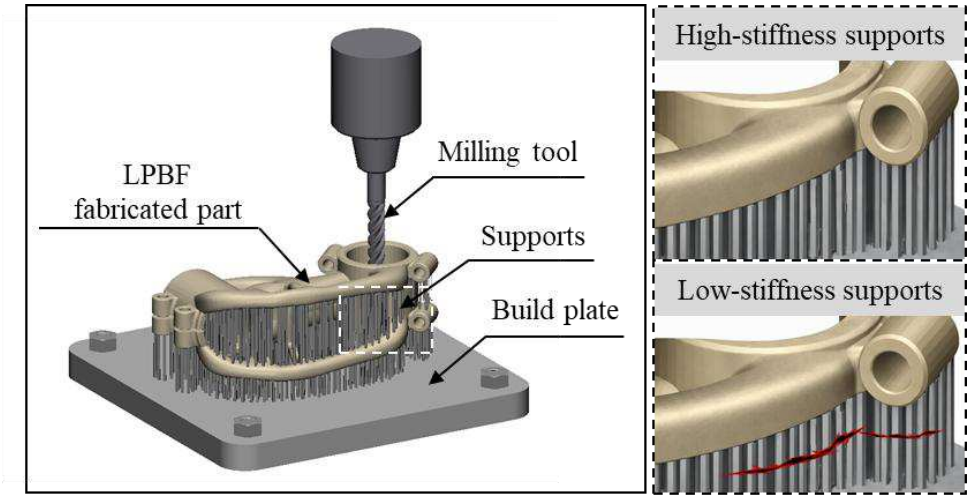


Fig. 1. Concept of support-assisted milling for additively manufactured parts using retained support structures as structural fixtures.

2. Material and methods

2.1 Fabrication of support-assisted milling specimens

To evaluate the feasibility of using as-built support structures as fixtures during milling, pure Ti Grade 2 specimens were fabricated via the LPBF process. The fabrication was carried out using an SLM 280 system (Nikon SLM Solutions).

LPBF-fabricated components may contain residual stresses induced by the rapid heating and cooling cycles inherent to the manufacturing process. Therefore, all specimens were subjected to stress-relief heat treatment to minimize the influence of residual stress. The as-built specimens were heat-treated at 590°C for 2 h under a vacuum of 1.9×10^{-5} Torr. Separate residual stress measurements confirmed that the residual stress level decreased from 560 MPa in the as-built condition to 146 MPa after heat treatment. Accordingly, all support-assisted milling experiments in this study were conducted using stress-relieved specimens.

All specimens were designed such that the part was connected to the build plate through support structures, forming an integrated part–build plate interface. Since the functional roles of the part region and the support structures are different, distinct LPBF process parameters were applied to each region during fabrication. The part region was fabricated with a layer thickness of 30 μm and a relatively high energy density to ensure mechanical properties and high density. In contrast, the support structures were fabricated using a layer thickness of 60 μm and a relatively lower energy density to improve productivity and facilitate subsequent removal. The detailed process parameters applied to each region are summarized in Table 1.

Two types of support structures commonly used in metal AM, namely block-type and rod-type supports, were designed and applied in this study. Fig. 2(a) illustrates the block-type support structure, where the lattice spacing was defined as the primary design variable. Fig. 2(b) shows the rod-type support structure, in which the pillar diameter was used as the design variable. The wall thickness of the support structures was fixed at 30 μm, as shown in Fig. 2(c), and the penetration depth of the support into the part was set to 120 μm to ensure structural connection between the support and the part. The design parameters applied to each support type are summarized in Table 2.

Table 1 LPBF process parameters applied to the part and support regions.

Parameters	Part	Support
Power [W]	170	150
Scan speed [mm/s]	900	650
Hatching space [mm]	0.12	0.12
Layer thickness [μm]	30	60

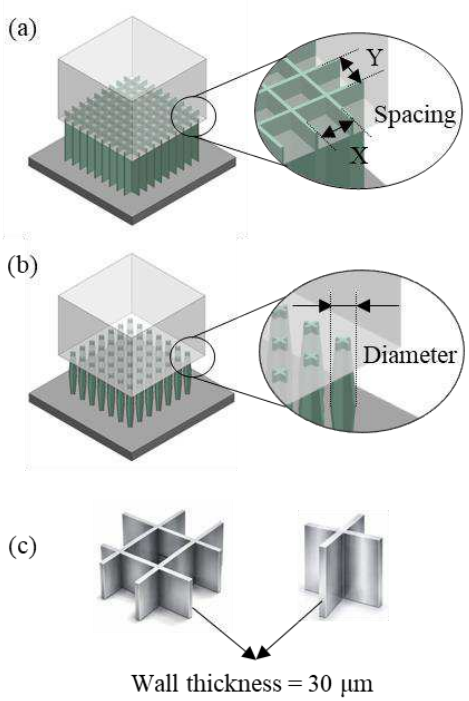


Fig. 2. Design parameters of the support structures: (a) definition of spacing in the block-type support, (b) definition of diameter in the rod-type support, and (c) wall thickness of the support structure.

Table 2 Design parameters and relative stiffness levels of different support types.

Specimen name	Geometry type	Parameter	Relative Stiffness
Block 1.0	Block	Spacing = 1.0 mm	Highest
Block 1.5	Block	Spacing = 1.5 mm	High
Rod 1.4	Rod	Diameter = 1.4 mm	Low
Rod 1.1	Rod	Diameter = 1.1 mm	Lowest

2.2 Cutting force measurement and modeling

To quantify cutting loads during milling, cutting force measurements were performed using bulk LPBF-fabricated pure Ti specimens. The milling experiments were conducted on a machining center (F600B, Hyundai Wia). A four-flute carbide end mill (GMH54060, YG-1) with a diameter of 6 mm was used as the cutting tool. Slot milling was performed under dry cutting conditions, and the spindle speed was set to 2000 rpm.

A total of nine machining conditions were tested by combining different depths of cut (DOC, a_p) and feed rates (v_f). Cutting forces under each condition were measured using a three-axis dynamometer (Kistler 9257B). The force signals were amplified using a charge amplifier and recorded through a data acquisition (DAQ) system, as illustrated in Fig. 3.

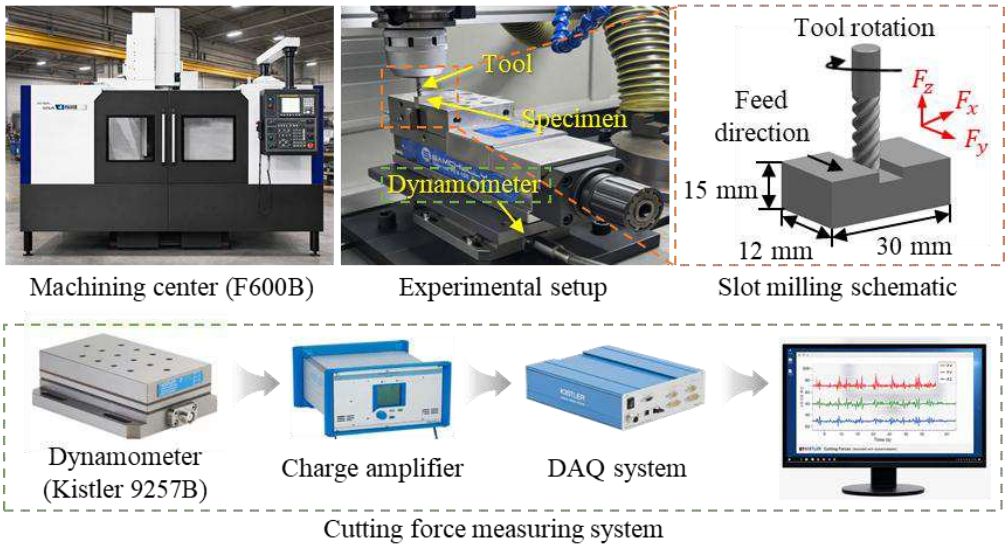


Fig. 3. Experimental setup for cutting force acquisition during milling experiments.

The experimental data were used to develop a cutting force model capable of calculating cutting forces under various machining conditions, which was subsequently used to estimate cutting loads in support-assisted milling and to provide input data for FEA.

In milling processes, cutting force is known to be closely related to the cutting cross-sectional area between the tool and the workpiece, and this relationship is widely used in mechanistic milling force models [22-25]. Under slot milling conditions, the average cutting cross-sectional area A_e can be defined as the product of the depth of

cut (DOC, a_p) and the feed per tooth f_z:

$$A_e = a_p \cdot f_z \tag{1}$$

The feed per tooth is calculated as:

$$f_z = \frac{v_f}{n \cdot z} \tag{2}$$

where n is the spindle speed and z is the number of cutter teeth.

Based on the mechanistic milling force model, which assumes that cutting force is proportional to the cutting cross-sectional area, the cutting force component in each direction F_i can be expressed as a linear relationship.

$$F_i = K_i A_e + C_i \ (i \in x, y, z) \tag{3}$$

where K_i represents the cutting force coefficient and C_i is a constant term. These coefficients were determined through linear regression analysis using the experimentally measured cutting force data, excluding the conditions in which tool breakage occurred.

The resulting cutting cross-sectional area-based model enables the estimation of cutting loads for combinations of DOC and feed rate that were not included in the experiments. The calculated cutting loads were subsequently used to determine milling conditions for the support-assisted specimens and were applied as directional cutting force components F_x, F_y, and F_z in the FEA.

Fig. 4 presents the experimentally measured cutting forces and the cutting force model obtained through regression analysis as a function of the cutting cross-sectional area. Fig. 4(a) shows the experimentally measured cutting force data, while Fig. 4(b) compares the experimental cutting forces with the cutting force model. The comparison shows good agreement, indicating that the model accurately reflects the experimentally measured cutting forces.

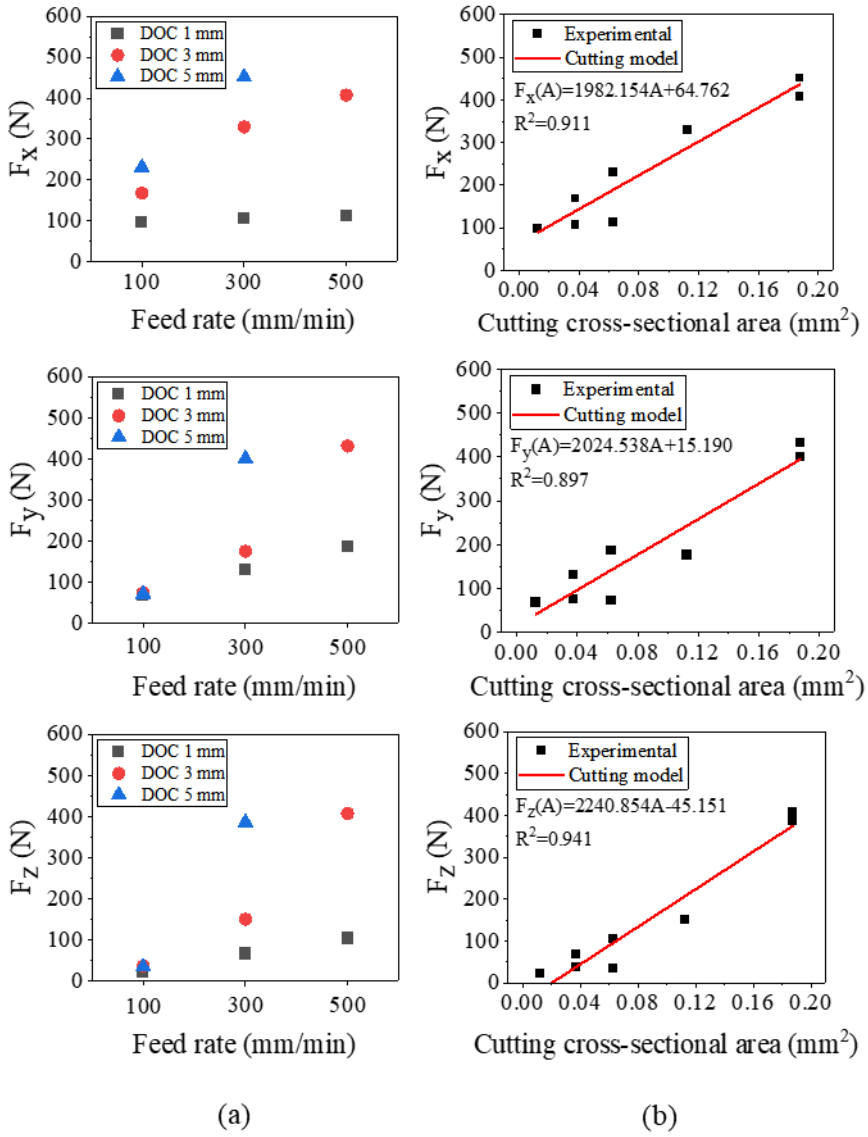


Fig. 4. (a) Experimental cutting forces measured under different DOC and feed rates. (b) Comparison between experimentally measured cutting forces and the cutting force model.

2.3 Support-assisted milling experiments

Support-assisted milling experiments were conducted to evaluate the feasibility of using support structures as structural fixtures during milling and to identify the critical machining conditions leading to support failure. The milling experiments were performed using a five-axis machining center (linear 20, DMG MORI). The critical machining conditions for support failure may vary depending on the stiffness of the support structure. Therefore, as shown in Fig. 5, the effective upper part length of the specimen was adjusted for each support type so that support failure could occur within a limited range of milling conditions.

Slot milling was performed for all specimens, and the machining conditions were selected to generate progressively increasing cutting loads. The cutting loads corresponding to each machining condition were estimated using the cutting cross-sectional area–based cutting force model described in Section 2.2. For each support type and machining condition, the milling experiments were repeated three times, and the results were presented as average values. During the milling experiments, support failure was monitored, and the machining condition at which failure occurred was defined as the critical machining condition.

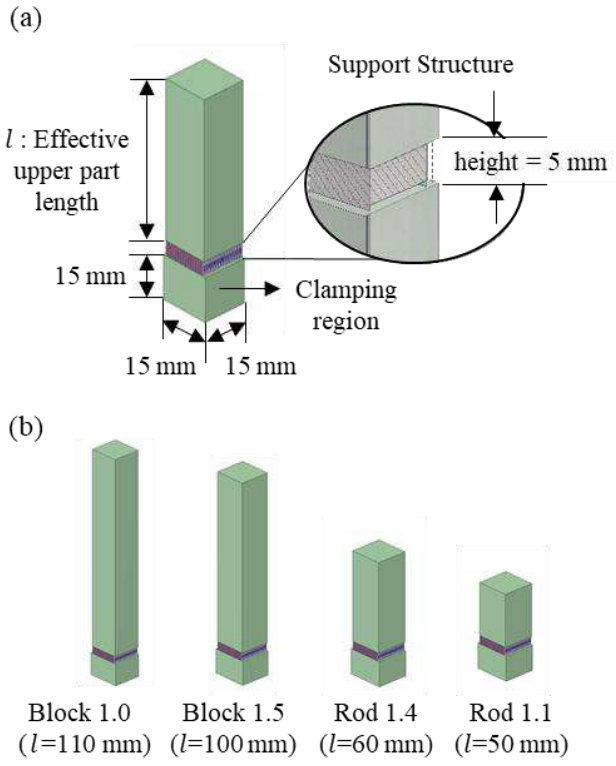


Fig. 5. (a) Design of the support-assisted milling specimen, and (b) variation in effective upper part length for different support types.

2.4 FEA model of the support structures

FEA was performed to quantitatively evaluate the stress distribution within the support structures during the support-assisted milling process. The simulations were conducted using ANSYS Workbench.

The analysis model consisted of an integrated structure including the upper machining part and the lower support structures. The bottom surface in contact with the build plate was defined as a fixed boundary condition, and the cutting load was applied as an external force acting on the machined surface. The external loading conditions were defined using the directional cutting force components F_x, F_y, and F_z, which were calculated from the cutting cross-sectional area–based force model.

The simulation results were analyzed based on the stress distribution at the interface between the support structures and the build plate. The cutting force applied to the top of the part structure predominantly induces a bending moment at the interface between the support structure and the build plate. At the edge of the support–build plate interface, where crack initiation is expected to occur, tensile stress is considered to be the dominant stress component governing crack initiation. Therefore, the maximum principal stress, which effectively represents the tensile stress state, was adopted as the failure criterion for evaluating support failure.

Since the actual support structures consist of periodic lattice or pillar-type geometries, a representative volume element (RVE) based approach was employed to replace the complex lattice structures with an equivalent material model suitable for numerical analysis [26-28].

First, the cross-sectional area of a fully solid structure was defined as the reference area. The actual cross-sectional area of each support type was then calculated, and the area ratio was defined as the actual area divided by the reference area. This area ratio was applied to the elastic modulus to assign an equivalent elastic modulus for each support type [26,29,30]. The calculated area ratios and corresponding equivalent elastic moduli for each support type are summarized in Table 3.

Table 3 Area ratio and equivalent elastic modulus assigned to each support type.

Support types	Area ratio	Elastic modulus [MPa]
Solid	1	115,000
Block 1.0	0.503	57,845
Block 1.5	0.335	38,525
Rod 1.4	0.285	32,798
Rod 1.1	0.216	24,840

2.5 Evaluation of machining quality under different stress levels

To investigate the influence of stress levels within the support structures on machining quality, machining quality evaluation was conducted. Straightness of the cutting path and surface roughness were selected as the primary evaluation metrics.

For the straightness evaluation, the slot milling path was divided into three regions: the entry region, steady-state region, and exit region, as illustrated in Fig. 6. The left and right wall dimensions measured in the steady-state region were defined as the reference values L_{steady} and R_{steady}, respectively. The corresponding left and right wall dimensions at the same positions in the entry and exit regions (L_{entry}, R_{entry}; L_{exit}, R_{exit}) were then measured. The straightness error was calculated based on the deviation from the reference values as follows:

$$\Delta entry = \frac{|L_{entry} - L_{steady}| + |R_{entry} - R_{steady}|}{2} \quad (4)$$

$$\Delta exit = \frac{|L_{entry} - L_{steady}| + |R_{entry} - R_{steady}|}{2} \quad (5)$$

Surface roughness was evaluated in the steady-state region along the cutting direction. The roughness parameters R_a and R_z were measured ten times, and the average values were used for evaluation.

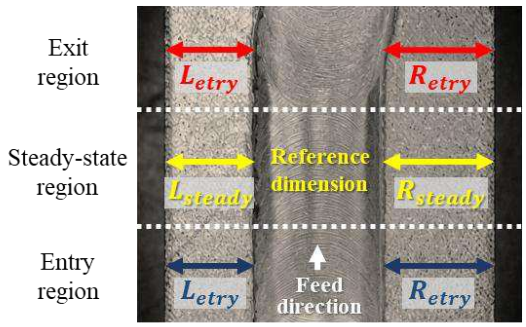


Fig. 6. Measurement method for evaluating straightness of the slot milling path.

3. Results and discussion

3.1 Support-assisted milling results

Support-assisted milling experiments were conducted under various machining conditions to evaluate the structural behavior of the support structures and the occurrence of support failure. For each support type, machining was performed with progressively increasing DOC and feed rate to increase the cutting force. The complete set of machining conditions and the corresponding failure results are summarized in Table 4.

In this study, the machining condition at which support failure occurred was defined as the critical machining condition for each support type. This condition represents the maximum allowable cutting condition that the support structure can sustain without structural failure. The experimental results show that the allowable cutting load varied significantly depending on the support stiffness. Even under identical machining conditions, the occurrence of support failure differed according to the support design.

Fig. 7 presents representative milling results for the Block 1.5 support type under conditions below and above the critical machining condition. When the machining condition remained below the critical level, the support structures maintained sufficient stiffness to provide stable support for the upper part during milling. In contrast, when the machining condition exceeded the critical machining condition, cracks initiated at the lower region of the support structures and subsequently propagated, leading to local delamination and fracture.

Table 4 Milling conditions and observed support failure results for different support types.

Case No.	Types of support	DOC [mm]	Feed rate [mm/min]	XYZ Resultant force [N]	Support failure
1	Block 1.0	3	150	279	Not Failed
2		3	200	348	Not Failed
3		3	250	416	Not Failed
4		3	300	485	Not Failed
5		3	330	526	Not Failed
6		3	340	540	Failed
7	Block 1.5	2	130	193	Not Failed
8		2	200	256	Not Failed
9		2	230	284	Not Failed
10		2	300	348	Not Failed
11		3	210	361	Not Failed
12		2	330	375	Failed
13	Rod 1.4	2	100	167	Not Failed
14		2	200	256	Not Failed
15		3	200	348	Not Failed
16		2	300	348	Not Failed
17		2	400	439	Not Failed
18		3	270	444	Failed
19	Rod 1.1	0.5	50	60	Not Failed
20		0.5	150	62	Not Failed
21		0.5	300	65	Not Failed
22		0.5	500	67	Not Failed
23		0.6	80	70	Not Failed
24		0.7	50	79	Failed

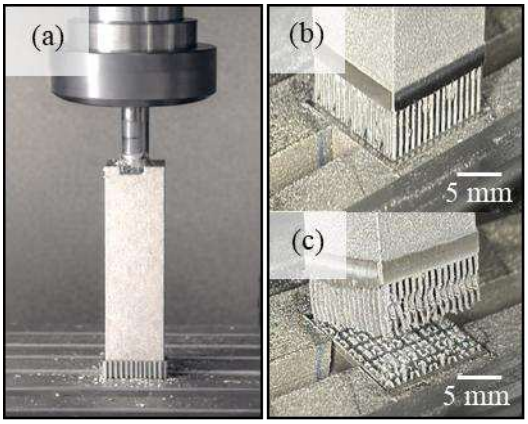


Fig. 7. Support-assisted milling results for the Block 1.5 specimens: (a) milling experiment configuration, (b) milling result under DOC 2 mm and feed rate 230 mm/min (below critical condition), and (c) milling result under DOC 3 mm and feed rate 280 mm/min (above critical condition).

3.2 Stress analysis of support structures based on FEA

The cutting loads corresponding to each machining condition were applied as external loading conditions in the FEA, and the maximum principal stress within the support structures was calculated for all machining conditions. The bottom surface in contact with the build plate was defined as a fixed boundary condition, while the cutting loads were applied to the machined surface.

Fig. 8 compares the distribution of maximum principal stress for the Block 1.0 specimen at a constant DOC of 3 mm under increasing feed rates. The maximum principal stress was concentrated along the outer edge of the interface between the support and the build plate. This location corresponded well with the crack initiation region observed in the milling experiments. In addition, the magnitude of the maximum principal stress increased progressively with increasing cutting load.

Table 5 summarizes the maximum principal stresses calculated for all machining conditions. For each support type, the maximum principal stress at which failure occurred in the experiments was defined as the critical stress of the support structure. Accordingly, the critical stresses were determined to be 401.7, 173.3, 102.2, and 79 MPa for the Block 1.0, Block 1.5, Rod 1.4, and Rod 1.1 support types, respectively. This critical maximum principal stress was subsequently used as the failure criterion for predicting support failure. In other words, when the maximum principal stress within the support structure exceeds this critical stress value, the likelihood of support failure significantly increases regardless of the specific machining parameters.

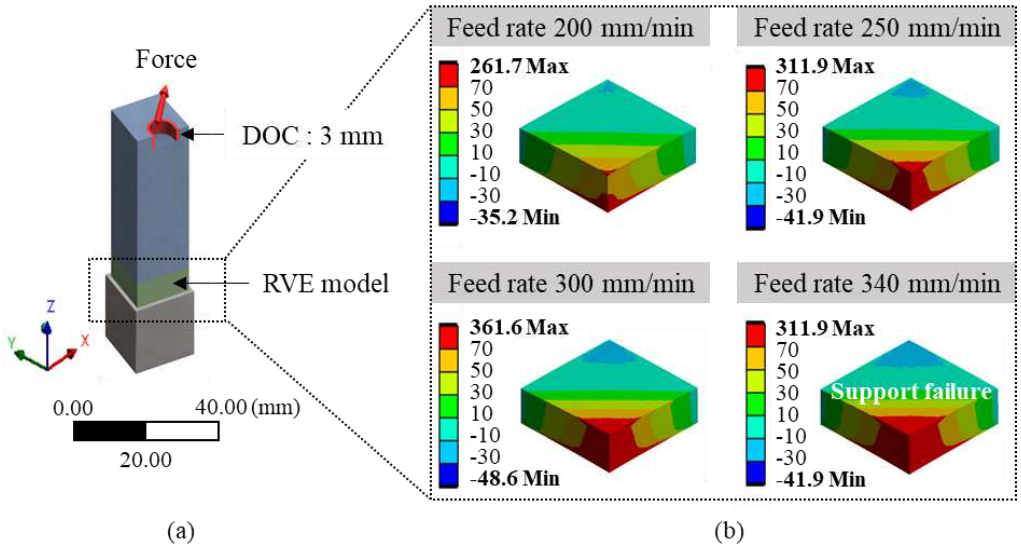


Fig. 8. (a) FEA model and loading condition, (b) distribution of maximum principal stress in the Block 1.0 specimen with varying feed rate at a constant DOC of 3 mm.

Table 5 Maximum principal stress calculated in the support structures for each machining condition.

Case No.	Max. principal stress [MPa]	Case No.	Max. principal stress [MPa]	Case No.	Max. principal stress [MPa]	Case No.	Max. principal stress [MPa]
1	211.9	7	91.8	13	40.0	19	60
2	261.6	8	120.4	14	60.8	20	62
3	311.3	9	132.6	15	80.6	21	65
4	361.6	10	160.8	16	81.3	22	67
5	390.9	11	166.6	17	102.2	23	70
6	401.7	12	173.3	18	102.2	24	79

3.3 Validation of support failure prediction using a cage geometry

To validate the practical applicability of the stress-based support failure prediction, milling experiments were conducted using a complex cage geometry fabricated on the same build plate. Two cage models were manufactured using LPBF, both employing the Block 1.5 support type. Slot milling was performed on the upper surface while retaining the support structures, with the specimen tilted to facilitate single-axis milling in the horizontal direction.

The critical stress for the Block 1.5 support structure determined from the previous experiments was 173 MPa. Therefore, two machining conditions were selected: one below the critical stress level and the other above it. Accordingly, milling was performed under these conditions: DOC = 2 mm with a feed rate of 230 mm/min, and DOC = 3 mm with a feed rate of 210 mm/min. The stresses applied to the support structures under these conditions were calculated to be 166 MPa and 205 MPa, respectively (Fig. 9).

Under the condition below the critical stress, stable cutting was achieved without any failure of the support structures. No noticeable deformation was observed on the machined upper surface, and detailed observations confirmed that no cracks or delamination occurred at the lower region of the supports or at the support–build plate interface.

In contrast, when the stress level exceeded the critical stress, cracks initiated at the support structures during machining and propagated along the loading direction. Localized failure of several support elements was observed, which resulted in a loss of machining stability.

These results experimentally demonstrate that the critical stress criterion derived from the specimen-based experiments can be effectively applied not only to simple test geometries but also to more complex cage structures. In particular, the results indicate that machining stability is governed primarily by the stress level within the support structures rather than by the machining parameters alone. Therefore, the stress-based machining condition design approach proposed in this study can serve as a quantitative guideline for process planning in which support structures are utilized as structural fixtures. The proposed framework provides a practical basis for predicting machining stability and selecting appropriate machining conditions in post-processing of LPBF-fabricated parts.

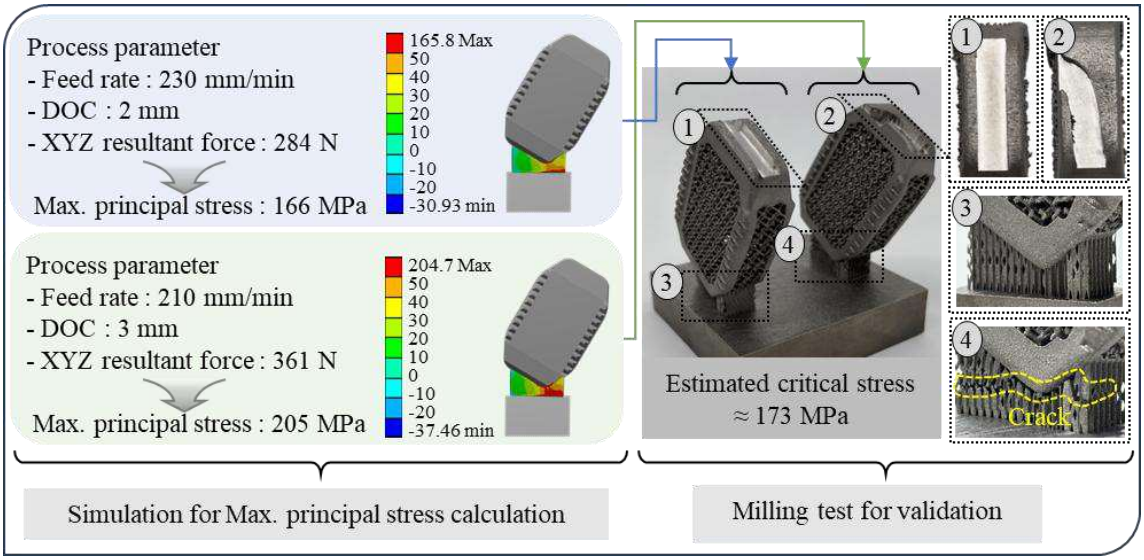


Fig. 9. Comparison of machining behavior below and above the critical stress in the cage geometry with Block 1.5 support structures.

3.4 Machining quality evaluation under different stress levels

To investigate the influence of stress levels in the support structures on machining quality, the machining results were compared by dividing the stress levels into three regions: below the critical stress ($\sigma<\sigma_{crit}$), near the critical stress ($\sigma\approx\sigma_{crit}$), and above the critical stress ($\sigma>\sigma_{crit}$). Fig. 10 presents representative slot milling results corresponding to each stress region. When the stress level remained below the critical stress, stable cutting was achieved. However, as the stress approached the critical level, the straightness of the cutting path gradually deteriorated. When the stress exceeded the critical value, support failure occurred and the specimen detached during machining, resulting in process interruption.

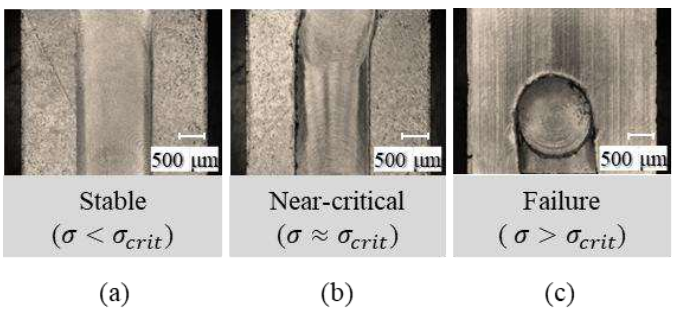


Fig. 10. Comparison of slot milling results under different maximum principal stress levels.

The straightness analysis results shown in Fig. 11 indicate that, for the block-type specimens, the straightness error in both the entry and exit regions increased progressively with increasing stress level. In particular, the straightness error in the exit region was larger than that in the entry region. This behavior can be attributed to the relatively longer upper part length of the block-type specimens, which leads to more pronounced bending deformation under cutting loads.

In contrast, for the rod-type specimens, although a certain level of straightness error was observed in both the entry and exit regions, the increase in straightness error with respect to stress level was less pronounced compared to the block-type specimens. This can be explained by the relatively shorter upper part length of the rod-type specimens, which results in smaller bending deformation under similar cutting loads. In other words, even when a similar stress or strain level is applied at the base of the support structures, an increase in specimen length leads to larger bending deformation, resulting in greater displacement of the machining region and consequently a deterioration in straightness quality. These results suggest that, in the design of post-machining processes, not only the occurrence of support failure but also the stress range that leads to machining quality degradation should be considered.

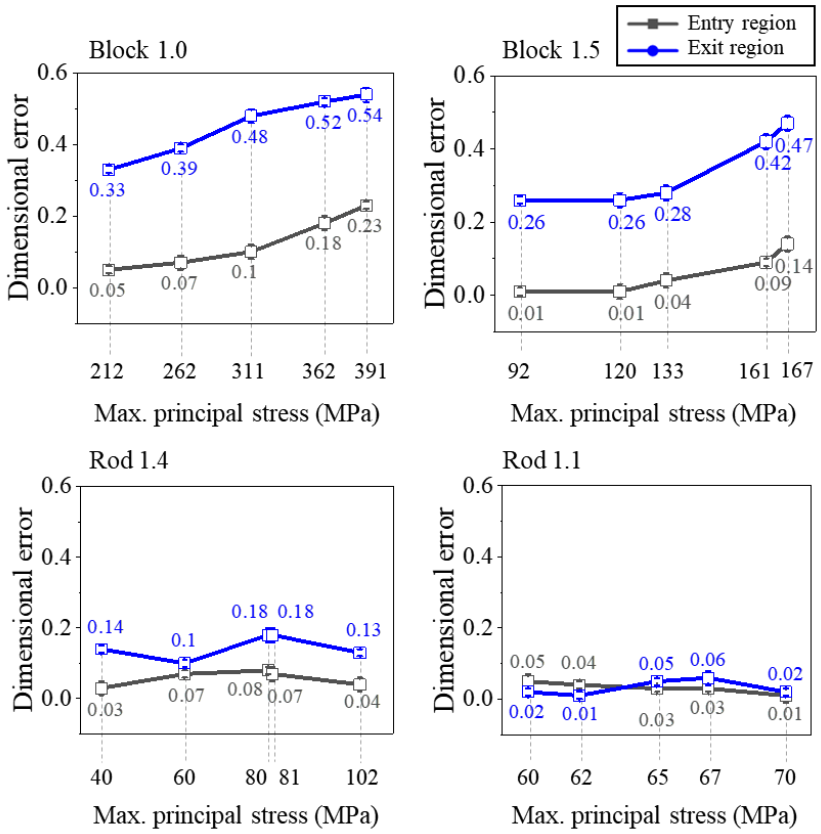


Fig. 11. Results of cutting path straightness evaluation under different stress levels.

To analyze the influence of increasing stress levels on the surface quality of the machined region, the surface roughness was measured under each machining condition, and the results are presented in Fig. 12. For all support configurations, both R_a and R_z exhibited a gradual increase as the stress level increased. This trend can be attributed to the increased fluctuation in the relative position between the tool and the workpiece under higher cutting loads. As the stress level increases, the structural deformation of the specimen becomes more pronounced, leading to slight variations in the tool–workpiece interaction during cutting. These micro-scale fluctuations are reflected in the machined surface as increased surface roughness.

The results indicate that increasing stress levels can directly lead to deterioration of surface quality. Moreover, the results suggest that changes in machining quality may occur even within the stress range where support failure does not occur.

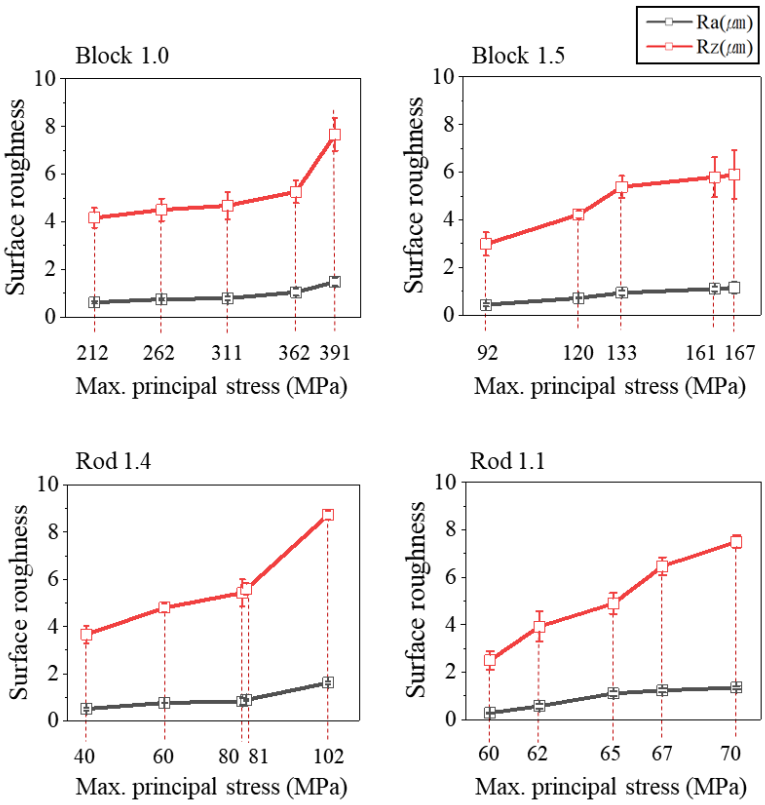


Fig. 12. Surface roughness results of the machined surface under different stress levels.

4. Conclusions

In this study, a stress-based approach was proposed to predict support failure and evaluate machining quality in support-assisted milling, where the support structures formed during the LPBF process are retained and utilized as structural supports during milling. The proposed approach was validated through a combination of experiments and FEA. The main findings are summarized as follows:

1. Cutting forces of LPBF-fabricated pure Ti Grade 2 were experimentally measured under various combinations of DOC and feed rate. Based on the relationship between cutting force and cutting cross-sectional area, a cutting load model was established, enabling the quantitative estimation of cutting loads under arbitrary machining conditions.
2. Milling experiments were conducted on specimens with integrated support structures by gradually increasing the cutting load. The machining condition at which support failure occurred was defined as the critical machining condition for each support type. The results showed that the allowable machining load range varied significantly depending on the support design.
3. The cutting loads predicted by the cutting force model were applied to FEA to evaluate the maximum principal stress within the support structures. Different support geometries and stiffness conditions resulted in different stress levels, and the stress corresponding to the experimentally observed failure condition was defined as the critical stress for each support type.
4. Support failure was found to initiate at the interface between the support structures and the build plate, where the maximum principal stress was concentrated. The predicted stress concentration region showed good agreement with the crack initiation locations observed in the milling experiments. Furthermore, validation experiments using a complex cage geometry confirmed that stable machining was achieved when the stress level remained below the critical stress, whereas support failure occurred when the stress exceeded this threshold.
5. Analysis of machining quality under different stress levels showed that straightness and surface roughness remained stable below the critical stress, while dimensional error and surface roughness gradually increased with increasing stress. These results indicate that stress levels influence machining quality even before the onset of support failure.

Overall, the proposed stress-based machining condition design approach provides a quantitative guideline for predicting support failure and machining stability in support-assisted milling of LPBF parts. The proposed

framework can be effectively utilized for process planning and machining condition selection in the post-processing of LPBF-fabricated components.

Funding Declaration

This study has been conducted with the support of the Korea Institute of Industrial Technology as " Development of Multi-modal Crack Monitoring AI Models for LPBF Process Based on Acoustic Emission and Layer-wise Images (KITECH JH-26-0009)".

Declaration of Competing Interest

The authors declare that they have no known competing financial interests or personal relationships that could have appeared to influence the work reported in this paper.

Acknowledgements

-

References

[1] I. Gibson, D. Rosen, B. Stucker, Additive Manufacturing Technologies, Springer, New York, 2015.

[2] T. DebRoy, H.L. Wei, J.S. Zuback, T. Mukherjee, J.W. Elmer, J.O. Milewski, A.M. Beese, A. Wilson-Heid, A. De, W. Zhang, Additive manufacturing of metallic components – Process, structure and properties, Progress in Materials Science 92 (2018) 112–224.

[3] A. Hussein, L. Hao, C. Yan, R. Everson, P. Young, Advanced lattice support structures for metal additive manufacturing, Journal of Materials Processing Technology 213 (2013) 1019–1026.

[4] W.E. King, A.T. Anderson, R.M. Ferencz, N.E. Hodge, C. Kamath, S.A. Khairallah, Overview of modelling and simulation of metal powder bed fusion process, Materials Science and Technology 31 (2015) 957–968.

[5] D. Herzog, V. Seyda, E. Wycisk, C. Emmelmann, Additive manufacturing of metals, Acta Materialia 117 (2016) 371–392.

[6] P. Mercelis, J.P. Kruth, Residual stresses in selective laser sintering and selective laser melting, Rapid Prototyping Journal 12 (2006) 254–265.

[7] X. Xu, Y. Li, Z. Wang, J. Liu, Y. Zhang, Laser additive manufacturing of titanium alloys: Process, materials and post-processing, Rare Metals 43 (2024) 6288–6328.

[8] Y. Kaynak, O. Kitay, The effect of machining on surface integrity of additively manufactured Ti-6Al-4V alloy, Journal of Manufacturing Processes 36 (2018) 125–134.

[9] J. Flynn, A. Shokrani, S.T. Newman, V. Dhokia, Hybrid additive and subtractive machine tools – Research and industrial developments, International Journal of Machine Tools and Manufacture 101 (2016) 79–101.

[10] E. Maleki, N. Shamsaei, A comprehensive study on the effects of surface post-processing on fatigue performance of additively manufactured AlSi10Mg: An augmented machine learning perspective on experimental observations, Additive Manufacturing 87 (2024) 104321.

[11] I.S. Jawahir, E. Brinksmeier, R. M'Saoubi, J. Aspinwall, J.C. Outeiro, D. Meyer, D. Umbrello, A. Jayal, Surface integrity in machining of additively manufactured metallic materials, CIRP Annals – Manufacturing Technology 65 (2016) 819–842.

[12] F. Calignano, Design optimization of supports for overhanging structures in aluminum and titanium alloys by selective laser melting, Journal of Materials Processing Technology 214 (2014) 203–213.

[13] J. Zhang, Q. Cao, W.F. Lu, A review on design and removal of support structures in metal additive manufacturing, Materials Today: Proceedings 70 (2022) 407–411.

[14] J. Vanek, J. Galicia, B. Benes, Clever support: Efficient support structure generation for digital fabrication, Computer Graphics Forum 33 (2014) 117–125.

[15] P. Didier, G. Le Coz, G. Robin, P. Lohmuller, B. Piotrowski, A. Moufki, P. Laheurte, Consideration of additive manufacturing supports for post-processing by end milling: A hybrid analytical–numerical model and experimental validation, Progress in Additive Manufacturing 7 (2022) 15–27.

[16] P. Didier, G. Le Coz, G. Robin, P. Lohmuller, A. Moufki, P. Laheurte, Consideration of SLM additive manufacturing supports on the stability of flexible structures in finish milling, Journal of Manufacturing Processes 62 (2021) 213–220.

[17] M. Höller, F. Klocke, B. Döbbeler, Direct machining of selective laser melted components with optimized support structures,*Procedia CIRP* 81 (2019) 375–380.

[18] Y. Zheng, Z. Zhao, B. Xu, Y. Yu, J. Xu, A method to predict chatter stability accurately in milling thin-walled parts by considering force-induced deformation, Journal of Manufacturing Processes 106 (2023) 552–563.

[19] O. Özşahin, Optimization of variable pitch milling tools for improved chatter stability, Journal of Manufacturing Processes 120 (2024) 260–271.

[20] M. Wang, G. Wang, P. Gao, J. Peng, Online building of milling stability lobe diagrams based on multi-feature signals, Journal of Manufacturing Processes 152 (2025) 458–476.

[21] Y. Zhang, H. Ding, L. Zhu, Stability prediction of milling process based on dynamic cutting force model and regenerative chatter analysis, Journal of Manufacturing Processes 64 (2021) 133–145.

[22] E. Budak, Y. Altintas, E.J.A. Armarego, Prediction of milling force coefficients from orthogonal cutting data, Journal of Manufacturing Science and Engineering 118 (1996) 216–224.

[23] M. Wan, W.H. Zhang, Y.C. Ma, An improved mechanistic cutting force model for milling process, International Journal of Machine Tools and Manufacture 50 (2010) 102–113.

[24] Y. Altintas, P. Lee, Mechanics and dynamics of ball end milling, Journal of Manufacturing Science and Engineering 120 (1998) 684–692.

[25] Y. Sun, Y.B. Guo, S.Y. Liang, Characteristics of cutting forces and chip formation in machining of titanium alloys, *International Journal of Machine Tools and Manufacture* 49 (2009) 561–568.

[26] L.J. Gibson, M.F. Ashby, Cellular Solids: Structure and Properties, Cambridge University Press, Cambridge, 1997.

[27] S. Hollister, N. Kikuchi, Homogenization theory and digital imaging, Biotechnology and Bioengineering 43 (1994) 586–596.

[28] V.S. Deshpande, N.A. Fleck, M.F. Ashby, Effective properties of the octet-truss lattice material, Journal of the Mechanics and Physics of Solids 49 (2001) 1747–1769.

[29] X. Yan, J. Hao, L. Zhao, Mechanical properties of lattice structures fabricated by selective laser melting, Materials & Design 84 (2015) 247–254.

[30] L. Dong, V.S. Deshpande, Mechanical response of metallic lattice structures, International Journal of Solids and Structures 78–79 (2016) 76–87.